mathematics

MDPI

Article

An Effective Analytical Approach to Predicting the Surface Contact Temperature of the Face Gear Drives

Jun Wen [1,2], Yuansheng Zhou [1,2,*], Jinyuan Tang [1,2] and Yu Dai [1,2]

[1] State Key Laboratory of Precision Manufacturing for Extreme Service Performance, Central South University, Changsha 410083, China; wenjun9528@csu.edu.cn (J.W.)
[2] College of Mechanical and Electrical Engineering, Central South University, Changsha 410083, China
* Correspondence: zyszby@csu.edu.cn

Abstract: The anti-scuffing bearing capacity of gears is a significant issue for their service lives, especially for the cases with heavy loads or high speeds. Generally, the anti-scuffing bearing capacity is evaluated according to the surface contact temperature that can be calculated with either analytical methods or finite element analysis (FEA) methods. The analytical methods usually apply the theory of Blok to efficiently obtain the results by simplifying some actual physical conditions, which are well considered in the FEA methods with accurate results but more computation time. Conversely, a new efficient and accurate analytical method is proposed by introducing the actual lubricant film thickness and continuous heat transfer for the theory of Blok. These two physical conditions are the key issues for the calculation of the two parts of surface contact temperature, flash temperature and bulk temperature, respectively. For the calculation of flash temperature, elastohydrodynamic lubrication (EHL) is introduced to consider the lubricant film thickness for the theory of Blok, and the result is obtained by solving the Reynolds equation efficiently with the finite difference method. For the bulk temperature, the result for a contacting point on the gear tooth surface is directly obtained according the theory of Blok, and the continuous heat transfer among the adjacent contacting points is considered with Gaussian heat morphology, which can accurately construct the bulk temperature field distribution in the contact region. The proposed method is validated as in good agreement with the FEA method and with less computation time.

Keywords: face gear; analytical approach; FEA method; contact temperature; anti-scuffing

MSC: 65Z05

Citation: Wen, J.; Zhou, Y.; Tang, J.; Dai, Y. An Effective Analytical Approach to Predicting the Surface Contact Temperature of the Face Gear Drives. *Mathematics* **2023**, *11*, 3087. https://doi.org/10.3390/math11143087

Academic Editor: Efstratios Tzirtzilakis

Received: 23 June 2023
Revised: 6 July 2023
Accepted: 10 July 2023
Published: 13 July 2023

1. Introduction

Face gear transmission is a relatively new transmission mode with several distinct advantages, such as a large transmission ratio, insensitivity of assembly errors in the axial direction, and compact structure in some specific applications. Due to those special characteristics, there are plenty of applications for face gear drives in industry, such as for electric power tools, fishing tools, robots, automobiles, and aerospace products.

Many scholars have produced many works about the design and manufacturing of face gears to promote their application in industry. Litvin et al. had great contributions to the systematic knowledge of face gears [1,2]. They focused on the application of face gear drives on helicopter transmission systems [3] by studying the modeling, tooth contact analysis (TCA), stress analysis, and manufacturing of face gears meshed with different types of pinions, such as involute spur pinions [4,5], helical spur pinions [6], asymmetric spur pinions [7], and worms [8]. Zhou et al. [9,10] studied the meshing and generation of face gears with the conical helical pinions. Liu et al. [11] established a model of eccentric face gear transmission for the study of gear transmission and tooth contact analysis. Wu et al. [12] proposed a CAD/CAE integration method for the generative design of face gears.

Zhou et al. [13] applied a new envelop approach to establish the closed-from representation of the tooth surface for the face gears meshed with general spur pinions or involute helical pinions. Different manufacturing approaches were well-investigated for the face gears, such as disk grinding [14–17], worm grinding [18], CNC milling [19], plunge milling [20], planning [21], shaving [22], honing [23].

When face gear drives are used in high-speed and heavy-load conditions, the frictional heat in the meshing process could cause a high temperature on the tooth surface. In a high-temperature condition, scuffing failure would present a high risk of damage to the gear teeth [24]. Hence, it is significant to investigate the surface contact temperature for those high-speed and heavy-load applications of face gears. Unfortunately, the topic of the surface contact temperature of the face gear is barely studied. To make this issue clear, a detailed review of the surface contact temperature of gears is implemented as follows.

Many scholars have studied the surface contact temperature for different gears, excepting face gears. Zhang et al. [25] and Gan et al. [26] investigated the temperature behavior of spiral bevel gears by finite element analysis (FEA), and they proposed a coupled thermo-elastic-hydrodynamic analysis to determine temperature rise. They found that, due to surface deformation, the high-temperature region shifts to the top of the tooth, and the maximum flash temperature occurs at the contact ellipse before the pitch point is engaged in the meshing process. Fernandes et al. [27] implemented an FEA thermal model to predict the bulk and flash temperature on polymer gears. They proposed a method for modeling the temperature rise and distribution along the tooth by using the capabilities of a gear power loss model. Li et al. [28] studied the tooth surface temperature field of helical gears by considering machining and installation errors. Mohammadpour et al. [29] applied thermal EHL analysis to study the influence of hybrid non-Newtonian thermoelastic fluid dynamics on hypoid gears under high contact loads and shear rates. Wang and Cheng [30] presented a direct method to investigate the surface contact temperature in spur gears based on one-dimensional transient heat conduction analysis under a semi-infinite plane. On this basis, Zhu and Cheng et al. [31] also studied the rise of surface contact temperature in point contacts. Bobach et al. [32] presented a model for calculating transient, three-dimensional, thermal-elastic-hydrodynamic tooth flank contacts in spur gears. This model considered mass-conserving cavitation, non-Newtonian flow, and the real involute characteristics of the tooth flanks. Li et al. [33] implemented the three-dimensional analysis of the unsteady-state temperature field and temperature sensitivity analysis to spur gears and investigated the varying transient thermal pattern of all nodes' temperatures in any engaging period.

According to the aforementioned review, the previous studies of tooth surface contact temperature focus on the spur gears, helical gear, and spiral bevel gears, but rarely face gears. For those studies, FEA methods are more popular than the analytical methods. One reason is that the FEA methods can effectively model the actual physical conditions, such as convective heat transfer, to obtain the accurate bulk temperature, which is usually approximately calculated by the analytical methods as an average value. According to many applications, the FEA method is an effective way to study the tooth surface contact temperatures of different gears; thus, it also works for face gears. However, the computation process of FEA methods is usually time-consuming, and the related commercial software as well as skillful technicians is needed. It would be great if an effective analytical method, which can accurately model the bulk temperature, were proposed to calculate the surface contact temperature of face gears, and the result should be close to that of the FEA method. Based on this idea, this work proposes a new analytical model of the tooth surface contact temperature with two main aspects. First, the flash temperature is analytically calculated according to the Blok flash temperature theory. Second, Gaussian distribution is used to describe the bulk temperature of the tooth surface.

The rest of the contents are organized as shown in Figure 1. In Section 2, we simply introduce the tooth surface representations of face gear drives and numerically obtain their TCA result according to the existing methods. These results are used in Section 3

to analytically calculate the flash temperature of the face gear tooth surface according to Blok flash temperature theory. In Section 4, Gaussian distribution is introduced to obtain the bulk temperature as an analytical result. Since the proposed method is related with analytical calculation rather than FEA methods, we name it as an analytical approach to differentiate with the FEA methods. In Section 5, the proposed analytical method is validated with FEA. Furthermore, the further investigation of the surface temperature is studied with the change in the geometric parameters of face gears. Conclusions are given at the end.

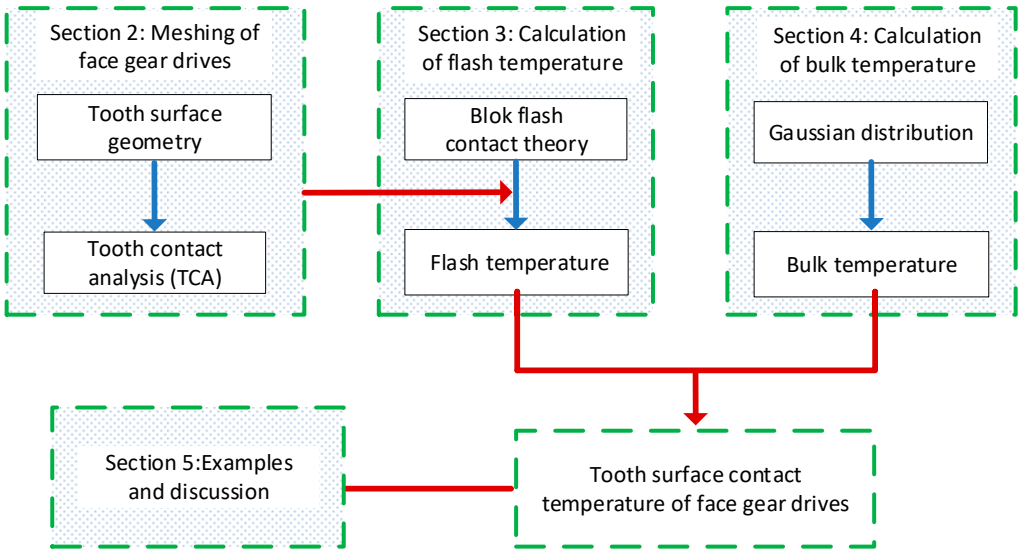

Figure 1. The flow chart of the organization of this work.

2. Meshing of Face Gear Drives

2.1. Tooth Surface Geometry of Face Gear Drives

As depicted in Figure 2, a face gear drive is composed of a face gear and a pinion. For design purposes, the pinion is replaced by a shaper, which has the same tooth surface parameters as the pinion except the tooth number. The tooth number of shapers is usually bigger than for pinions to achieve the point contact between the meshing of the face gear and pinion [1]. The tooth surface of the face gear is designed based on the meshing process between the shaper and face gear. It includes a working part and a fillet part. The working part is generated as the envelope surface of the shaper tooth surface, and the fillet part is generated as the swept surface of the top edge of the shaper tooth surface. Geometrically, only the working part takes part in the meshing process, which is related to our topic of 'surface contact temperature'. Hence, only the working part of the face gear tooth is investigated in this work, and the fillet part is not discussed.

In the meshing process, assume that rotation angles for the face gear and shaper are assigned as ϕ_2 and ϕ_s, respectively. The index '2' is a conventional subscript for the face gear, while '1' and '*s*' are used for the pinion and shaper, respectively. ϕ_2 and ϕ_s are related as [1]

$$\frac{\phi_2}{\phi_s} = \frac{N_s}{N_2} \tag{1}$$

where N_2 and N_s are the tooth numbers of the face gear and the shaper, respectively. Assume that S_2 and S_s are the coordinate systems fixed to the face gear and shaper, respectively, and the homogenous transformation matrix from S_s and S_2 is represented as $\mathbf{M}_{2s}$. Based on the meshing process, the working part of face gear tooth surface is calculated as the

envelope surface to the family surfaces of the shaper tooth surface. Subsequently, it is represented as [1]

$$\begin{cases} \begin{bmatrix} \mathbf{r}_2(u_s, v_s, \phi_s) \\ 0 \end{bmatrix} = \mathbf{M}_{2s}(\phi_s) \cdot \begin{bmatrix} \mathbf{r}_s(u_s, v_s) \\ 0 \end{bmatrix} \\ \mathbf{n}(u_s, v_s) \cdot \mathbf{v}(u_s, v_s, \phi_s) = 0 \end{cases} \tag{2}$$

The first equation in Equation (2) calculates the family surfaces of the shaper tooth surface. u_s and v_s are two surface parameters of the shaper tooth surface. $\mathbf{r}_s(u_s, v_s)$ and $\mathbf{r}_2(u_s, v_s, \phi_s)$ are the representations of the shaper surface in S_s and the family surfaces in S_2, respectively. The second equation of Equation (2) is the equation of meshing, according to which one parameter among u_s, v_s and ϕ_s can be eliminated. **n** and **v** are the normal of the shaper tooth surface and velocity of the shaper tooth surface relative to the face gear. According to Equation (2), the tooth surface of the different face gears can be calculated when $\mathbf{r}_s$ and $\mathbf{M}_{2s}$ are given. Usually, one surface parameter of the shaper tooth surface is eliminated, and the tooth surface of the face gear is represented with respect to the other two parameters. To make it simple, here, we write the expression of the tooth surface of the face gears in S_2 as $\mathbf{r}_2(u_2, v_2)$, where u_2 and v_2 are two surface parameters of the face gears used in the rest of this work. The details of the calculation can be referred to in the previous works, such as Litvin's work. In particular, the closed-form (explicit) representations of the face gears meshed with the spur pinions or standard involute helical pinions are obtained in Zhou et al. [13].

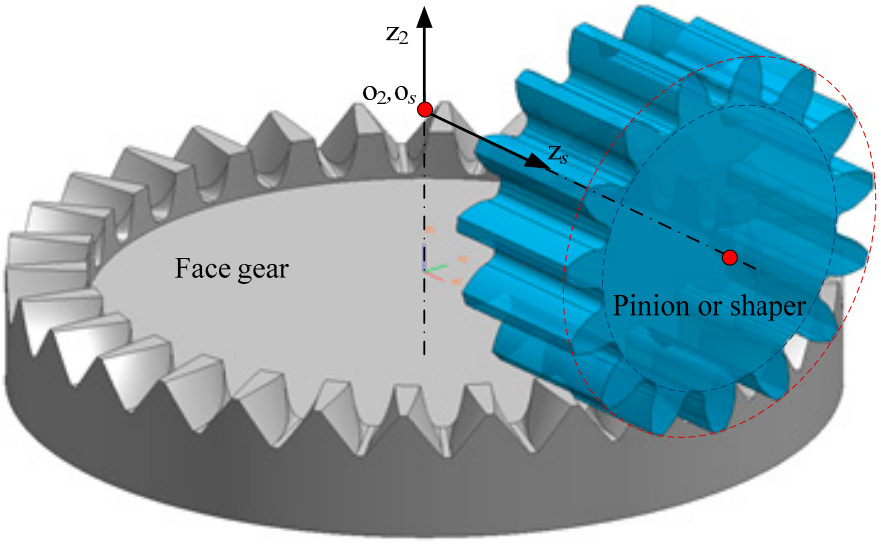

Figure 2. The meshing of a face gear drives.

With the representation of the face gear tooth surface, the curvatures of the face gear tooth surface can be calculated as the preliminary work for the calculation of the surface contact temperature. For a point on the face gear tooth surface, if a given direction $d\mathbf{r}$ on the tangent plane to this point is given as

$$d\mathbf{r} = \mathbf{r}_u du + \mathbf{r}_v dv \tag{3}$$

where $\mathbf{r}_u$ and $\mathbf{r}_v$ are the partial derivatives, and $\mathbf{r}_u d_u$ and $\mathbf{r}_v d_v$ are two decompositions of $d\mathbf{r}$ along $\mathbf{r}_u$ and $\mathbf{r}_v$, respectively, the normal curvature along $d\mathbf{r}$ is calculated as [1]

$$\kappa_n = \frac{Ldu^2 + 2Mdudv + Ndv^2}{Edu^2 + FMdudv + Gdv^2} \tag{4}$$

where E, F, G, L, M, and N are the coefficients. Furthermore, the principal curvatures are calculated as [1]

$$\kappa_{1,2} = H \pm \sqrt{H^2 - K} \tag{5}$$

where H and K are the mean curvature and Gaussian curvature, and they are given as

$$\begin{cases} H = \frac{G \cdot L - 2 \cdot F \cdot M + E \cdot N}{2 \cdot (E \cdot G - F^2)} \\ K = \frac{L \cdot N - M^2}{E \cdot G - F^2} \end{cases} \tag{6}$$

2.2. TCA of Face Gear Drives

If both the face gear and pinion are rigid bodies, they theoretically contact at a point at a moment during the meshing process, as shown in Figure 3. Practically, this contact point will be deformed as an area named the contact ellipse, of which the semi-major axis b will be applied to analytically calculate the surface contact temperature later. By connecting all contact points during the meshing process, the contact path is obtained. Usually, TCA is investigated to calculate the contact points and contact path, and the contact point is further used to calculate the flash temperature. In particular, a general case is studied by considering the assembly errors, as shown in Figure 4. Coordinate systems S_1 and S_2 are attached to the pinion and the face gear, respectively. S_f and S_e are fixed coordinate systems corresponding to the frame. S_q, S_d, and S_e are auxiliary coordinate systems introduced for the simulation of installment errors including $\Delta\gamma_m$, ΔE, and Δq, and they are the error of the shaft angle, the offset of the pinion, and the axial displacement of the face gear, respectively.

Based on the meshing process, the contact point on the tooth surface of the face gear has the same position vector and unit normal vector as the contact point on the tooth surface of the pinion.

$$\begin{cases} \mathbf{M}_{f1}(\varphi_1) \cdot \begin{bmatrix} \mathbf{r}_1(u_1, v_1) \\ 1 \end{bmatrix} = \mathbf{M}_{f2}(\varphi_2) \cdot \begin{bmatrix} \mathbf{r}_2(u_2, v_2) \\ 1 \end{bmatrix} \\ \mathbf{M}_{f1}(\varphi_1) \cdot \begin{bmatrix} \mathbf{n}_1(u_1, v_1) \\ 1 \end{bmatrix} = \mathbf{M}_{f2}(\varphi_2) \cdot \begin{bmatrix} \mathbf{n}_2(u_2, v_2) \\ 1 \end{bmatrix} \end{cases} \tag{7}$$

where the superscript '1′ and '2′ are assigned to the pinion and face gear, the subscript 'f' represents coordinate system S_f, and φ_1 and φ_2 are the angles of rotation of the pinion and the face gear. As depicted in Figure 4, the transformation matrix $\mathbf{M}_{f1}$ from S_1 to S_f and the transformation matrix $\mathbf{M}_{f2}$ from S_2 to S_f are represented as

$$\mathbf{M}_{f1} = \begin{bmatrix} \cos\varphi_1 & -\sin\varphi_1 & 0 & 0 \\ \sin\varphi_1 & \cos\varphi_1 & 0 & 0 \\ 0 & 0 & 1 & 0 \\ 0 & 0 & 0 & 1 \end{bmatrix} \tag{8}$$

$$\begin{aligned} \mathbf{M}_{f2} &= \mathbf{M}_{fq}\mathbf{M}_{qd}\mathbf{M}_{de}\mathbf{M}_{e2} \\ &= \begin{bmatrix} \cos\varphi_2 & -\sin\varphi_2 & 0 & \Delta E \\ \cos(\gamma_m + \Delta\gamma)\sin\varphi_2 & \cos(\gamma_m + \Delta\gamma)\cos\varphi_2 & \sin(\gamma_m + \Delta\gamma) & B + \Delta q \sin(\gamma_m + \Delta\gamma) \\ -\sin(\gamma_m + \Delta\gamma)\sin\varphi_2 & -\sin(\gamma_m + \Delta\gamma)\cos\varphi_2 & \cos(\gamma_m + \Delta\gamma) & \Delta q \cos(\gamma_m + \Delta\gamma) + B\cot\gamma_m \\ 0 & 0 & 0 & 1 \end{bmatrix} \end{aligned} \tag{9}$$

Equation (7) yields a system of scalar equations with six unknown variables as

$$\begin{cases} \boldsymbol{r}_{fx}^{(1)}(u_1, v_1, \varphi_1) = \boldsymbol{r}_{fx}^{(2)}(u_2, v_2, \varphi_2) \\ \boldsymbol{r}_{fy}^{(1)}(u_1, v_1, \varphi_1) = \boldsymbol{r}_{fy}^{(2)}(u_2, v_2, \varphi_2) \\ \boldsymbol{r}_{fz}^{(1)}(u_1, v_1, \varphi_1) = \boldsymbol{r}_{fz}^{(2)}(u_2, v_2, \varphi_2) \\ n_{fx}^{(1)}(u_1, \varphi_1) = n_{fx}^{(2)}(u_2, \varphi_2) \\ n_{fy}^{(1)}(u_1, \varphi_1) = n_{fy}^{(2)}(u_2, \varphi_2) \\ n_{fz}^{(1)}(u_1, \varphi_1) = n_{fz}^{(2)}(u_2, \varphi_2) \end{cases} \tag{10}$$

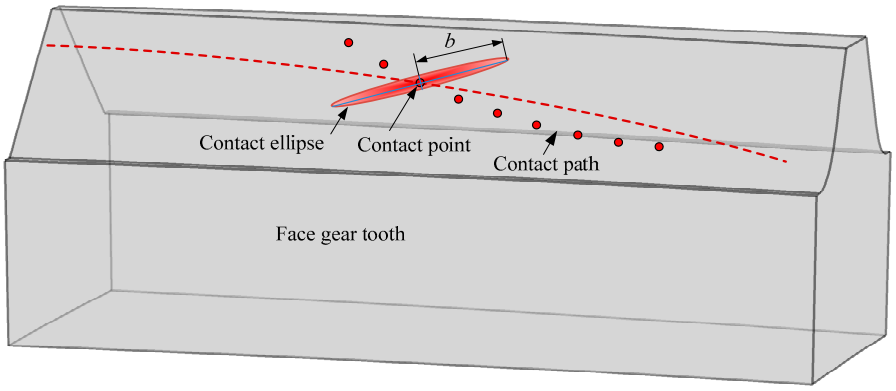

Figure 3. Schematic diagram of the contact path of the face gears.

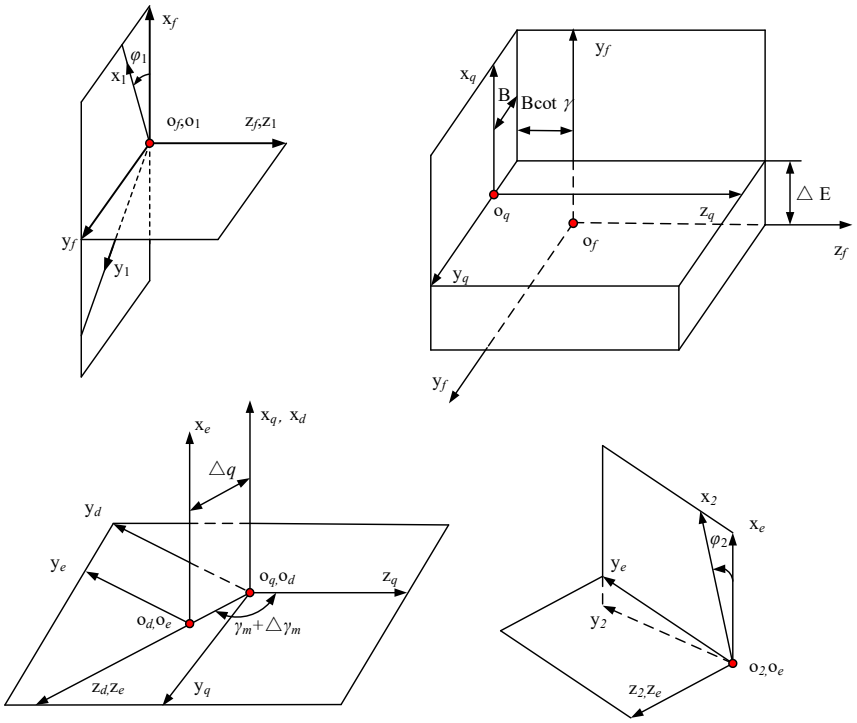

Figure 4. Coordinate system and assembly errors for the TCA face gear drives.

It is worthwhile mentioning that Equation (10) has only five independent scalar equations because both sides of the second equation of Equation (7) are unit-normal. For the meshing process, we can choose variable φ_1 as the input one, so that Equation (10) can be solved with five unknown variables and five independent scalar equations. Subsequently, the contact path of the face gear drive can be obtained. Furthermore, the

curvature information at each contact point on the contact path can also be obtained according to knowledge of differential geometry, as stated in Equations (3)–(6). With the curvature information, the shape of the contact ellipse can be calculated [1].

On the basis of the tooth surface geometry and TCA of the face gear drives, a tooth surface contact temperature solution model can be established. The Figure 1 is presented to express the solution procedure more directly. The surface contact temperature of the face gear teeth consists of two parts, which are the bulk temperature and the instantaneous flash temperature produced from the frictional heat during the meshing process [34]. The detailed calculation method of the flash temperature and the bulk temperature of the face gear will be discussed below.

3. Calculation of Flash Temperature

During the meshing process, the tooth surface flash temperature is the instantaneous temperature generated at the instantaneous contact point along the contact path. The flash temperature can be analytically calculated according to the flash temperature formula of Blok [34]. This method is successfully applied in cylindrical gears and bevel and hypoid gears. Since the face gear drives are very similar to the hypoid gear drives, here it is also applied to calculate the tooth surface flash temperature of face gear drives. According to the flash temperature formula of Blok [34,35], the flash temperature is calculated as

$$\theta_{\mathrm{fla}} = 1.11 \frac{\mu F_{\mathrm{n}} |v_{\mathrm{t1}} - v_{\mathrm{t2}}|}{\sqrt{2b}(B_1\sqrt{v_{\mathrm{t1}}} + B_2\sqrt{v_{\mathrm{t2}}})} \tag{11}$$

where θ_{fla} is the flash temperature of the contact point; μ is friction coefficient; F_{n} is the normal load; v_{t1} and v_{t2} are the values of the tangential velocities of the pinion and the face gear at the contact point, respectively; B_1 and B_2 are the thermal contact coefficient of the pinion and face gear respectively; and b is the half-width of the Hertz contact band, and it is equal to the length of the semi-major axis of the contact ellipse, as shown in Figure 3.

3.1. The Calculation of F_n and μ

Under lubrication conditions, taking full account of the special form of movement of the face gear drives, the friction coefficient and normal load of the tooth surface can be solved by mixed EHL analysis [36–38].

The applied normal load is the pressure integral in the contact area of the tooth surface [37].

$$F_{\mathrm{n}} = \iint_{\Omega} P(x,y)\mathrm{d}x\mathrm{d}y \tag{12}$$

$$P = \begin{cases} P_h, & h > h_{cr} \\ P_a, & 0 < h < h_{cr} \end{cases} \tag{13}$$

The oil film pressure causes elastic deformation of the contact surface and the film thickness is also controlled by the local geometry. The equation for calculating the film thickness when tooth surface roughness is not considered is expressed as [39]

$$h(x,y) = h_0 + \frac{x^2}{2R_{\mathrm{x}}} + \frac{y^2}{2R_{\mathrm{y}}} + V(x,y) \tag{14}$$

where h_0 represents the center distance of the two contact rigid bodies, R_{x} is the radius of curvature in the direction of the minor axis of the contact ellipse, R_{y} is the radius of curvature in the direction of the major axis of the contact ellipse, and V is the amount of elastic deformation of the contact surface.

The elastic deformation of the contact tooth surface is calculated by the Boussinesq integral at point of contact, which is expressed as [26]

$$V(x,y) = \frac{2}{\pi E^*} \iint_{\Omega} \frac{p(\xi,\zeta)}{\sqrt{(x-\xi)^2 + (y-\zeta)^2}} \mathrm{d}\xi \mathrm{d}\zeta \tag{15}$$

where E^* is the effective elastic modulus.

The pressure in the entire contact zone is governed by the Reynolds equation, expressed as

$$\frac{\partial}{\partial x}\left(\frac{\rho}{12\eta^*}h^3\frac{\partial p}{\partial x}\right) + \frac{\partial}{\partial y}\left(\frac{\rho}{12\eta^*}h^3\frac{\partial p}{\partial y}\right) = U_e\cos(\theta_e)\frac{\partial(\rho h)}{\partial x} + U_e\sin(\theta_e)\frac{\partial(\rho h)}{\partial y} \tag{16}$$

where ρ is the density, h is the oil film thickness between the interfaces, p is the pressure, and η^* is the effective viscosity of the lubricating oil.

In the contact area of the tooth surface, the contact surface pressure is generally hydrodynamic pressure, but, when the thickness of the lubricating oil film is less than a critical thickness, the asperities of rough surface come into contact directly, and the pressure becomes the solid asperities' contact pressure. The tooth surface friction coefficient can be obtained by solving for the normal pressure and shear stress of the tooth surface under different lubricant film thicknesses by the Reynolds equation.

Assuming a special case, when the left term of the Reynolds equation is 0, that is, when the thickness of the lubricating oil film is lower than a critical value (a typical value is taken as 10 nm), the pressure of the lubricating fluid is 0, and Reynolds equation can be simplified as the following form [37]

$$U_e\cos(\theta_e)\frac{\partial(\rho h)}{\partial x} + U_e\sin(\theta_e)\frac{\partial(\rho h)}{\partial y} = 0 \tag{17}$$

The simplified Reynolds equation is solved using the finite difference method with a first-order backward differencing format of

$$U_e\cos(\theta_e)\frac{\rho_{i,j}h_{i,j} - \rho_{i-1,j}h_{i-1,j}}{\Delta x} + U_e\sin(\theta_e)\frac{\rho_{i,j}h_{i,j} - \rho_{i,j-1}h_{i,j-1}}{\Delta y} = 0 \tag{18}$$

Considering the non-Newtonian properties of the lubricant, the effective dynamic viscosity used in the Reynolds equation is expressed as

$$\frac{1}{\eta^*} = \frac{1}{\eta}\frac{\tau_0}{\tau_L}\sinh\left(\frac{\tau_L}{\tau_0}\right) \tag{19}$$

where η is lubricant viscosity, τ_0 is a reference shear stress, and τ_L is the limiting shear stress.

The density of the lubricating oil also varies with the pressure, and its relationship with the pressure is as follows:

$$\rho = \rho_0\left(1 + \frac{0.6\times10^{-9}P}{1 + 1.7\times10^{-9}P}\right) \tag{20}$$

For the solution of the friction coefficient, the shear stress must be obtained first. According to the Ree-Eyring rheological model [40], the shearing stress is calculated using the following formula when the film thickness exceeds the critical value.

$$\gamma = \frac{\tau_0}{\eta}\sinh\left(\frac{\tau}{\tau_0}\right) \tag{21}$$

where γ is the shear rate of lubricant, which is usually a constant.

When the film thickness is below the critical value in the contact area, the asperities of the rough surface will be in direct contact and the shear stress can be calculated as

$$\tau_a(x,y) = p_a(x,y) \times f_c \tag{22}$$

where f_c is boundary friction, which changes with the surface roughness.

So far, the shear stress and the mixed traction force can be written as [41]

$$\tau = \begin{cases} \tau_h, & h > h_{cr} \\ \tau_a, & 0 < h < h_{cr} \end{cases} \tag{23}$$

$$F_f = \iint_{\Omega} \tau(x,y)\mathrm{d}x\mathrm{d}y \tag{24}$$

According to the above theory, the friction coefficient of the contact area of the face gear during meshing can be obtained.

$$\mu = \frac{F_f}{F_\mathrm{n}} = \frac{\iint_{\Omega} \tau(x,y)\mathrm{d}x\mathrm{d}y}{\iint_{\Omega} P(x,y)\mathrm{d}x\mathrm{d}y} \tag{25}$$

3.2. The Calculation of B_1 and B_2

In the face gear meshing transmission process, since the relative velocity and the radius of curvature of each contact position are different, the normal load and the friction coefficient are varied. The determination of the coefficient of friction is significant for the solution of the contact temperature. Since the rotational speed in the gear transmission is very high, a slight change in the friction coefficient also causes a large change in the contact temperature. In this paper, the mixed elastohydrodynamic lubrication model is used to solve for the normal load and friction coefficient in the BLOK flash temperature formula of the strip-shaped Hertzian contact, so that the calculation of the contact temperature of the gear at each contact point is more reasonable and accurate.

The contact temperature is affected by the thermal conductivity, density, and unit mass of the material. Therefore, the thermal contact coefficient between the tooth surfaces has to be taken into account. The thermal contact coefficient formula of the face gear and pinion is [35]

$$B_i = \left(0.001\lambda_i \cdot \rho_i \cdot c_i\right)^{1/2}, i = 1,2 \tag{26}$$

where B_i is the thermal contact coefficient, in $\mathrm{N/(mm^{1/2}{\cdot}m^{1/2}{\cdot}s^{1/2}{\cdot}K)}$; i = 1 represents the pinion gear and i = 2 represents the face gear; λ is the heat transfer coefficient of the gear material, in $\mathrm{N/(s{\cdot}K)}$; ρ is the density of the gear material, in $\mathrm{kg/m^3}$; and c is the specific heat per unit mass of the gear material, in $\mathrm{J/(kg{\cdot}K)}$.

The main curvature of the tooth profile of the face gear and the pinion at the meshing point and its corresponding main direction can be calculated from the face gear TCA. Where k_{21} and k_{22} are the principal curvatures of the face gear, k_{11} and k_{12} are the principal curvatures of the pinion. The angle between the main direction of the pinion and the major axis of the contact ellipse is α; the angle between the pinion and the first main direction of the face gear is σ. Therefore, the radii of curvature ξ_1 and ξ_2 of the pinion and the face gear in the direction of the major axis of the ellipse at the meshing point can be obtained.

$$\begin{cases} \xi_1 = \frac{1}{k_{11}\cos^2\alpha + k_{12}\sin^2\alpha} \\ \xi_2 = \frac{1}{k_{21}\cos^2(\alpha+\sigma) + k_{22}\sin^2(\alpha+\sigma)} \end{cases} \tag{27}$$

Since the convex surface of the pinion is in contact with the concave surface of the face gear, the comprehensive radius of curvature ξ at the contact point is

$$\xi = \frac{\xi_1 \xi_2}{\xi_2 - \xi_1} \tag{28}$$

4. Calculation of Bulk Temperature

In many periodic physical processes, such as gear meshing, bearing rolling, and metal cutting, a relatively stable thermal field is generated, and the heat generated will have a certain distribution pattern in a certain area. The classical thermal model has the rectangular thermal model proposed by JAEGER [42] and the derived triangular thermal model.

During the meshing of the gears, the contact temperature includes the flash temperature and the bulk temperature, as shown in Figure 5. Taking a pair of teeth for study, the flash temperature only occurs during the period in which it is meshing-in and meshing-out. The flash temperature at this time plus the body temperature is the contact temperature. When the teeth are not engaged, the tooth surface is in contact with the air and lubricating oil in the environment, and the surface temperature is the bulk temperature field. The face gear is a high-speed transmission mechanism with a very short cycle. In one operating cycle, the rate of change in the tooth surface bulk temperature is almost negligible with respect to the rotational frequency of the gear, so the bulk temperature of the tooth surface is a relatively stable temperature field.

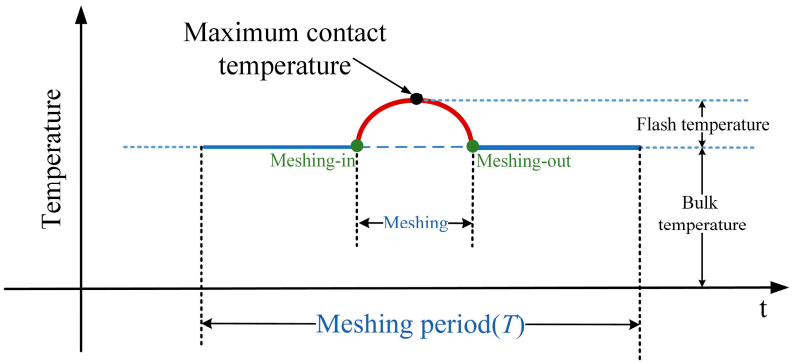

Figure 5. Contact temperature composition diagram.

For the calculation of the tooth surface temperature, a rough approximation calculation method is given in the BLOK theory, and its value can be calculated as [35]

$$\theta_m = \theta_{oil} + 0.47 \cdot X_S \cdot \frac{\int_A^B \theta_{fla} d\Gamma}{\Gamma_A - \Gamma_B} \tag{29}$$

where θ_{oil} is the operating temperature of lubricating oil and X_S is a coefficient defined according to the lubrication conditions as

$$X_S = \begin{cases} 1.2 & \text{spray lubrication} \\ 1.0 & \text{dip lubrication} \\ 0.2 & \text{submerged condition} \end{cases} \tag{30}$$

X_S = 1.2 for spray lubrication, X_S = 1.0 for dip lubrication, and X_S = 0.2 for gears submerged in oil, provided sufficient cooling.

The bulk temperature calculated by this method is a fixed value, so the body temperature of the tooth surface is a rectangular temperature profile. However, the lubrication conditions and heat dissipation conditions of the tooth surface, the tooth tip, and the root are different during the gear meshing process. In the finite element calculation of the tooth surface contact temperature, different convective heat transfer coefficients are usually

given to different tooth surfaces to simulate the different cooling conditions of the tooth surface [43]. However, in the numerical calculation of the tooth surface contact temperature, the contact temperature of the meshing region is calculated based on TCA and LTCA, and the influence of different cooling conditions outside the contact region and the convective heat transfer on the temperature of the contact region is not considered. Therefore, based on a large number of actual calculations, this paper proposes a Gaussian function optimization of the tooth surface bulk temperature field distribution, as shown in Figure 6. During the meshing process of a pair of teeth, since there is a large space in the tooth gap to store the lubricating oil, the convective cooling condition at the top and the root is better than that at the center of the tooth surface. Thus, a Gaussian distribution function is used to describe the tooth surface body temperature with good consistency. This hypothesis was verified by comparing the analytical approach results with the FEA results later in the paper.

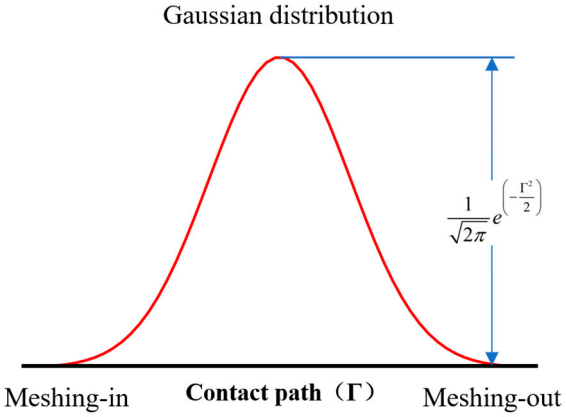

Figure 6. Gaussian distribution of bulk temperature.

The meshing position on the contact path is controlled by the dimensionless parameter Γ. The bulk temperature on the contact path and the surface contact temperature is expressed as

$$\theta_{\mathrm{b}} = K_a \theta_{\mathrm{m}} \frac{1}{\sqrt{2\pi}} e^{\left(-\frac{\Gamma^2}{2}\right)} \tag{31}$$

$$\theta = \theta_{\mathrm{fla}} + \theta_{\mathrm{b}} \tag{32}$$

where θ_{m} is the surface contact temperature, θ_{b} is the bulk temperature, and K_a is the temperature coefficient associated with gear material and lubricant parameters.

According to the above theoretical analysis, an analytical approach is established to achieve a fast solution for the surface contact temperature of the face gear.

5. Examples and Discussion

According to the theoretical solution derivation of the surface contact temperature of the face gear, a calculation process is programmed using a MATLAB script and a GUI interface is created to achieve fast solutions. The input modules in the software (Face gear tooth surface contact temperature calculation software V1.0) include the basic geometric parameters of the gears, the working conditions, the material parameters of the face gears and pinions, and the number of meshing points. The initial default parameters will be given in the input module, and the user can adjust the parameters according to the actual requirements. For example, by adjusting the basic geometric parameters of the gears, it is possible to calculate the contact temperature not only for the conventional design of the face gears but also for the face gears after the tooth surface has been reshaped. The number of meshing points indicates the number of discrete points on the contact path. The greater the number of discrete points, the more accurate the calculation result, but, at the same time, it reduces the calculation efficiency. Through multiple calculations, it

was found that 50 discrete points can have the best calculation efficiency with guaranteed calculation accuracy. Therefore, the default number of discrete points is set to 50, which can be increased if necessary to obtain a smoother calculation curve. The output modules of the software include the contact temperature, the contact path calculated by the TCA, and an assessment of the risk of scuffing. After entering the parameters in the input module and clicking the "Start" button, the calculation result can be quickly obtained, as shown in Figure 7. Integrating the face gear TCA with the contact temperature solution and forming software can achieve a fast and efficient solution. The comparison of the computational efficiency of the FEA and the presented approach is shown in Table 1. The results show that the computational speed of the analytical approach is about 67 times faster than that of FEA.

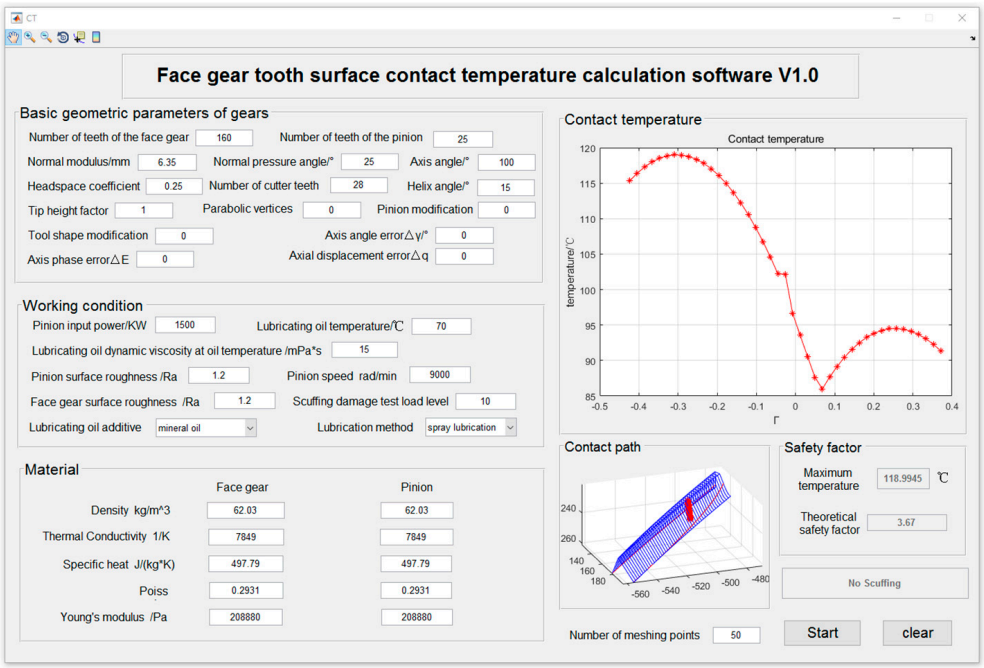

Figure 7. Face gear tooth surface contact temperature calculation software (° is the unit of angle).

Table 1. Computation time.

Method	Time
Finite element analysis	16 min 28 s
Analytical approach	14.72 s

5.1. Calculation Example

According to the established surface contact temperature solution model, the surface contact temperature of a typical face gear is calculated. The basic geometric parameters of the face gear and the paired pinion are shown in Table 2. The transmission conditions are shown in Table 3.

According to the parameters in Table 2, the face gear modeling and TCA solution are performed, and the face gear single-tooth model and the contact path can be obtained, as shown in Figure 8. Then, the operating conditions of the face gear are determined by the parameters in Table 3, and the surface contact temperature of the face gear along the contact path can be calculated, as shown in Figure 9.

Table 2. Geometry parameters of a typical face gear.

Factors	Face Gear
Number of teeth	160
Module (mm)	6.35
Pressure angle (°)	25
Helix angle (°)	15
Shaft angle (°)	100
Tooth width (mm)	75
Tooth height coefficient	1
Headspace coefficient	0.25

Table 3. Working parameters of a typical face gear pair.

Input power (kW)	1500
Pinion speed (r/min)	9000
Material of gears	SA E9310steel
Ambient viscosity of lubricant (mPa·s)	15
Ambient density of lubricant (kg/m^3)	870
Reference shear stress of lubricant (MPa)	0.15

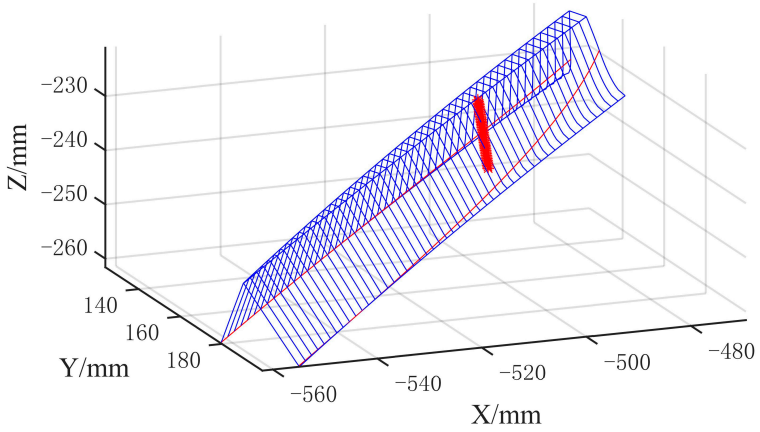

Figure 8. Face gear numerical model and tooth surface contact path.

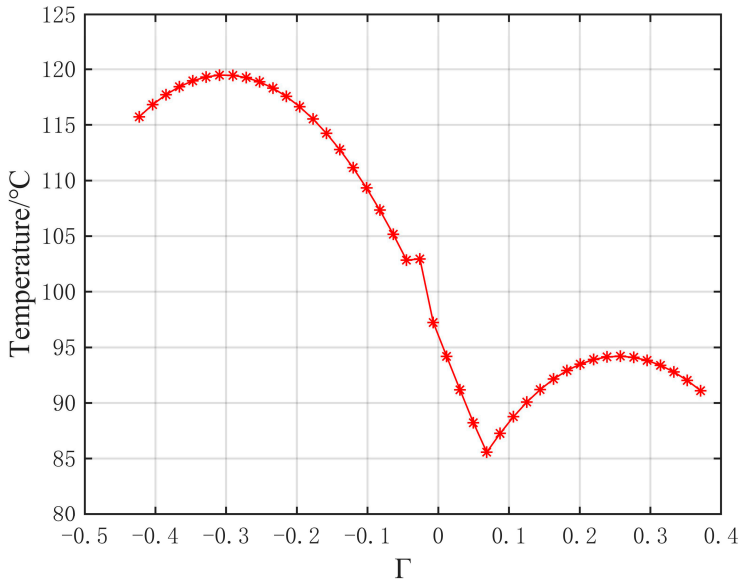

Figure 9. Temperature distribution along the contact path.

As depicted in Figure 9, the maximum surface contact temperature is 118.9 °C, and its position appears near the top of the tooth. The minimum contact is 85.6 °C, which appears near the pitch point of the mesh line. This is because the relative speed of the face gear and the small wheel is relatively high when the meshing is just entered, but the relative velocity near the pitch point tends to zero. Larger relative velocities produce greater frictional heat, causing an instantaneous temperature rise.

5.2. Finite Element Calculation Comparison

In order to verify the correctness of the analytical model of the created surface gear flash temperature, the same face gear geometry and transmission conditions were used to calculate the tooth surface contact temperature in the FEA. The model of a face gear drive with a helical pinion is shown in Figure 10. In one operating cycle of the face gear drive, each pair of teeth performs only one meshing motion. After the operation of the face gear is stabilized, the working cycle of each pair of teeth is very short due to the high rotational speed, so the change in the contact temperature value on each pair of teeth is very close. Therefore, one of the face gears is selected to calculate the surface contact temperature when it is engaged. In the finite element calculation, a heat source intensity is added to the face gear meshing area to simulate the energy flowing into the face gear during the meshing process; thereby, the temperature field distribution of the face gear tooth face is solved. The approximate heat flux on contact ellipse of face gear can be obtained as

$$Q(x,y) = \frac{1}{2}\mu(x,y) \times P(x,y) \times v_{\mathrm{t}}(x,y) \tag{33}$$

where Q is the heat flux distribution on face gear surface and v_{t} is the relative sliding velocity between meshing surface.

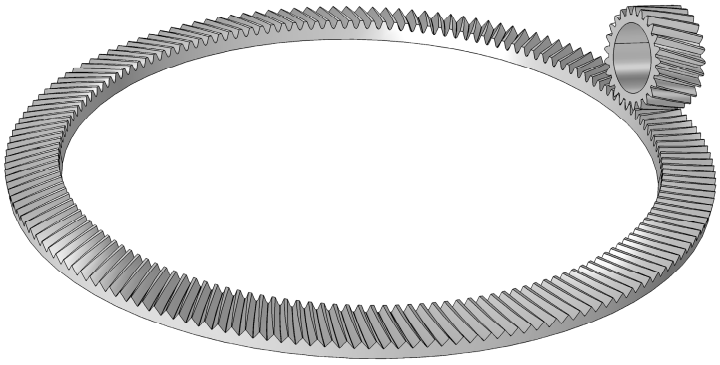

Figure 10. Face gear drives with a helical pinion.

Using the FEA method to solve the distribution of the tooth surface temperature field requires determining the convective heat transfer coefficient between the gear faces and the lubricating oil. Assume that the convection heat flow of each face is parallel to the normal of the face. Therefore, the Nusselt number of each face can be determined, and then the convective heat transfer coefficient of each face can be obtained according to Equation (33) [44].

$$H_i = \frac{Nu_i \times \lambda}{L} \tag{34}$$

where H_i is the convection heat transfer coefficient, Nu_i is the Nusselt number, λ is the thermal conductivity of fluid, and L is the characteristic length of boundary surface.

In this paper, COMSOL Multiphysics 6.0 commercial finite element software is used to solve for the temperature field. Since the temperature variation on each tooth is the same in the stable operating condition of the face gear drive, one face gear pair is selected for the presentation of the results. Heat flux is added as boundary conditions in the meshing

area, and the corresponding convective heat transfer coefficient is set at different boundary surfaces. The simulation results are shown in Figure 11.

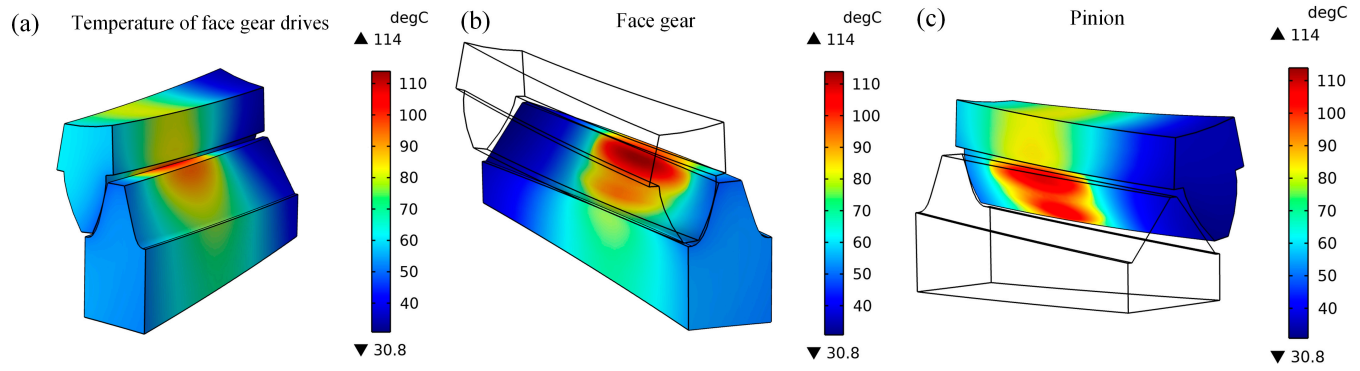

Figure 11. Tooth surface contact temperature field distribution: (**a**) contact temperature of the face gear drives; (**b**) contact temperature of the face gear; (**c**) contact temperature of the pinion.

It can be seen from the simulation results that, in the temperature profile of the face gear, the high-temperature region is concentrated in the region between the pitch line and the tooth tip. From the tip to the root of the tooth, the temperature first decreases and then increases, and it reaches a minimum surface contact temperature near the pitch line. In order to further explore the difference between the FEA result and the analytical approach calculation result, the temperature value on the tooth surface contact line in the finite element calculation result is compared with the analytical approach calculation result, as shown in Figure 12, which shows the temperature fluctuation from the crest to the root of the contact path.

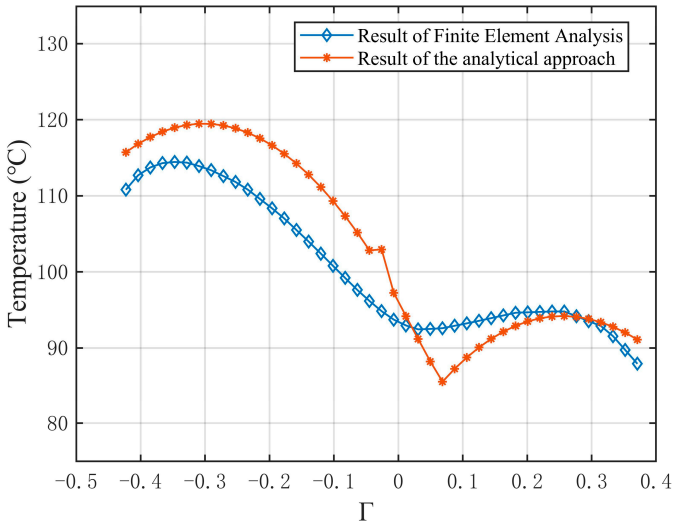

Figure 12. Comparison of analytical results which are optimized by a Gaussian distribution with finite element analysis (FEA) results.

The results of the analytical approach and the finite element calculation result show a good consistency. The maximum surface contact temperature calculated by the analytical approach is found to be 118.9 °C, the maximum temperature calculated by the FEA method is 114 °C, and the error is only 4.3%. By comparing the error of other contact positions, it can be found that the maximum temperature difference between the two calculation results occurs at the position of $\Gamma = -0.1$; the temperature difference is 9.2 °C, and the error is 9.1%. Therefore, it is proved that the analytical approach proposed in this paper has better accuracy while achieving a fast solution.

In Section 4 of the paper, it is mentioned that it is more reasonable and accurate to use the Gaussian distribution to describe the bulk temperature field of the gear surface. In order to verify this hypothesis, the constant bulk temperature value is directly used in the analytical method to calculate the tooth surface meshing temperature and compared with the finite element calculation result, as shown in Figure 13. Compared with the results calculated using the Gaussian distribution bulk temperature, the contact temperature curve calculated using the constant bulk temperature has a more significant error from the finite element calculation result. The specific performance is as follows: (1) The temperature change from the crest to the root of the gear surface is directly reduced and then increased, and does not show the temperature fluctuations of the finite element calculation results. (2) In terms of numerical value, it also has a large error with the finite element calculation result, especially in the interval from pitch point to root. At the root position, the calculation error of the two reached 22.3%, which exceeded the error range of the engineering calculation. It can be seen that using the Gaussian function to optimize the bulk temperature is beneficial to improve the calculation accuracy of the contact temperature.

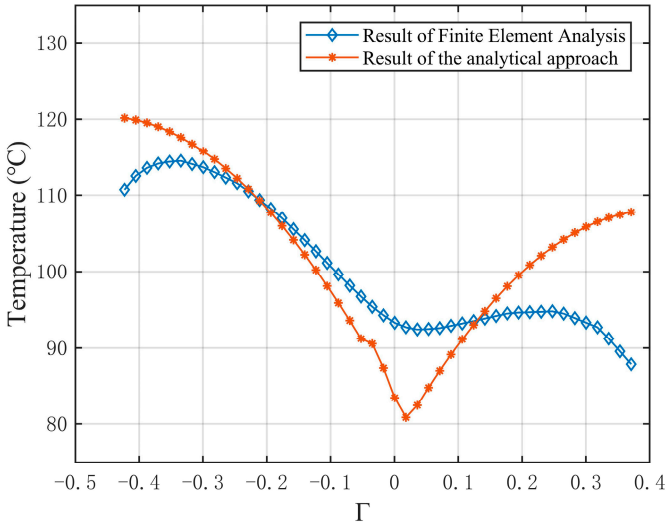

Figure 13. Comparison of analytical results which use constant bulk temperature with FEA results.

5.3. Effect of Geometric Parameters of the Face Gear on the Surface Contact Temperature

In the design of the face gear, different geometric parameters can construct different tooth profiles. The difference of the geometric profile of the tooth surface will show the difference of the coincidence degree, the relative tangential speed, and the contact area in the face gear transmission. These differences are more pronounced when the face gear is rotating at high speed. In order to study the influence of different geometric parameters on the surface contact temperature of the face gear, the pressure angle, helix angle, shaft angle and tooth width in Table 2 were separately changed to discuss their influence on the surface contact temperature of the tooth surface, as shown in Figure 14.

The tooth surface contact temperature can be significantly reduced by increasing the pressure angle. This is because the increase in the pressure angle can reduce the component of the contact force in the normal direction of the tooth surface, but the increase in the pressure angle causes a decrease in the degree of coincidence, so that the contact area of the tooth surface becomes small. Increasing the helix angle or increasing the shaft angle can reduce the surface contact temperature near the root region, and can also bring the lowest surface contact temperature of the tooth surface toward the root. However, the surface contact temperature at the top of the tooth is not sensitive to helix angle and shaft angle. This is because helix angle and shaft angle can change the position of the contact area on the tooth surface, but they do not change the range of the contact area. The change in tooth

width has the least effect on the surface contact temperature because the effect of the change in tooth width on the shape of the involute profile of the tooth surface is not significant.

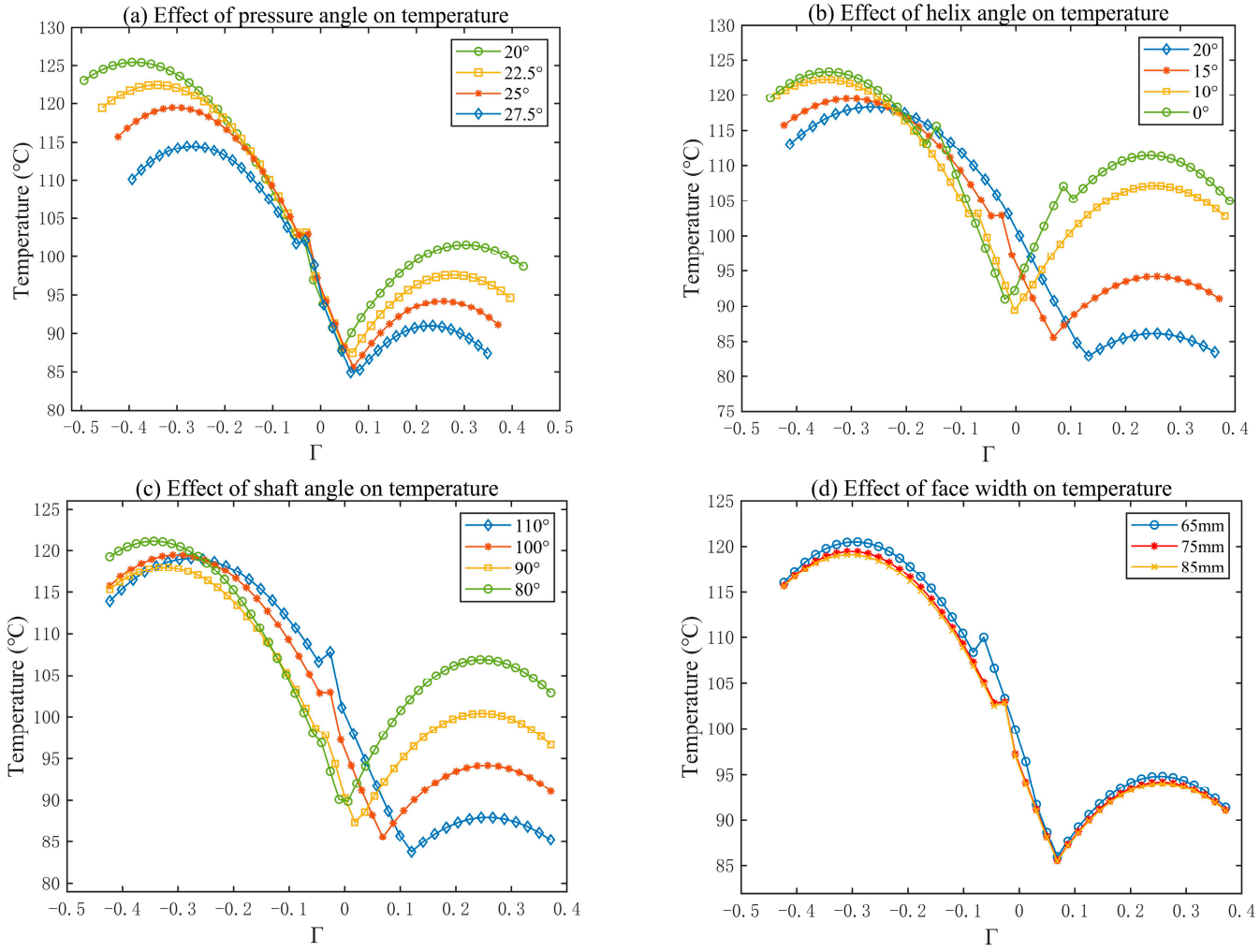

Figure 14. Influence of different geometric parameters on surface contact temperature: (**a**) effect of pressure angle on temperature; (**b**) effect of helix angle on temperature; (**c**) effect of shaft angle on temperature; (**d**) effect on face width on temperature.

When the helix angle of the face gear and the pinion is 90°, that is, when the pinion is a spur gear, the transmission mechanism formed by them becomes a face gear drive with a spur pinion transmission mechanism as show in Figure 15, which is a special form of the face gear transmission. As can be seen in Figure 14, in the spur gear–face gear transmission pair, the contact temperature of the surface is greater than that of the face gear drives with helical pinion transmission mechanisms, so further research on the face gear drives with spur pinion transmission mechanisms is required. The helix angle in the basic geometric parameters of the face gear and the pinion is set to 90° and remains unchanged, and then the pressure angle and the shaft angle are respectively set as unique variables in the calculation of the tooth surface contact temperature. Figure 16 is a calculation result of the contact temperature at different pressure angles. Figure 17 is a calculation result of the contact temperature at different shaft angles.

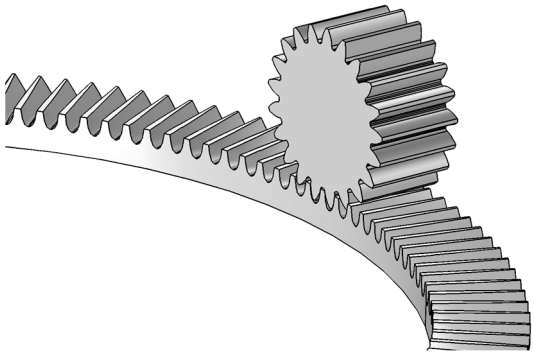

Figure 15. Face gear drives with a spur pinion.

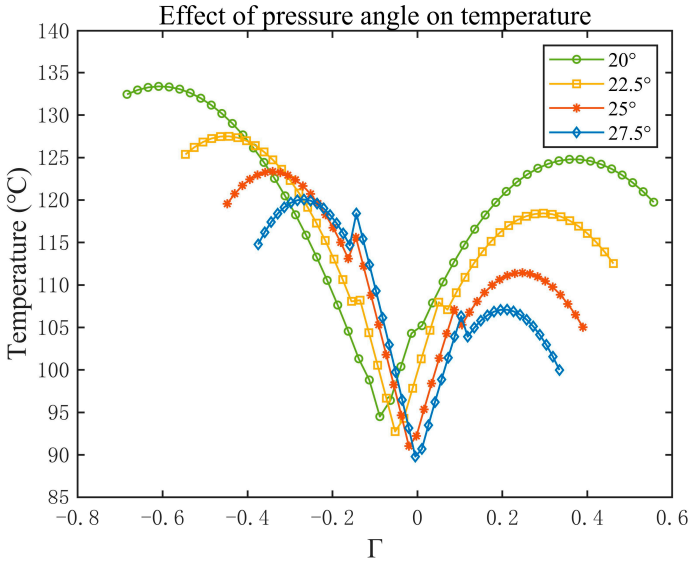

Figure 16. The result of the contact temperature at different pressure angles.

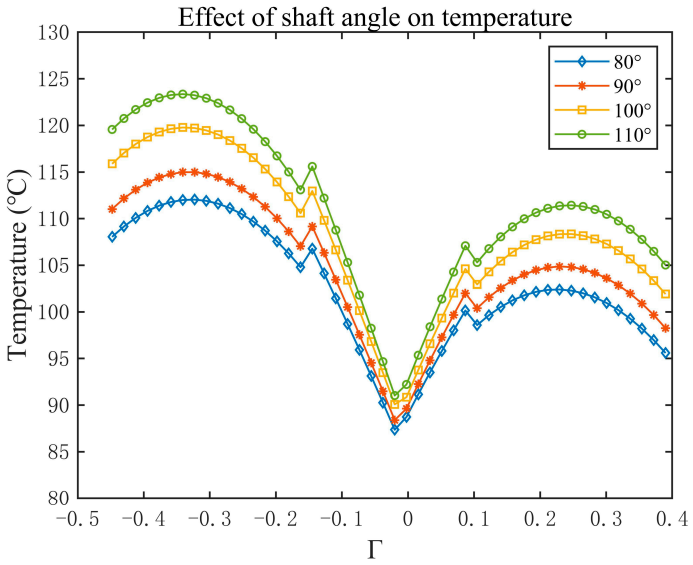

Figure 17. Result of the contact temperature at different shaft angles.

In the face gear drive with a spur pinion, as with the face gear drive with a helical pinion, the pressure angle causes a change in the contact arc length. As the pressure angle decreases, the meshing area on the tooth surface increases, so the contact arc length

is also longer. However, as the pressure angle decreases, the contact force between the tooth surfaces increases, and, as a result, the tooth surface contact temperature rises as the pressure angle decreases. Comparing the sensitivity of the face gear drive with a spur pinion and the face gear drive with a helical pinion to the pressure angle, it can be found that the face gear drive with a spur pinion is more sensitive to changes in the pressure angle. Changing the same value of the pressure angle will make the change in the position of the contact area on the face gear drive with a spur pinion more significant, and, at the same pressure angle, the contact temperature of the face gear drive with a spur pinion is greater than the contact temperature of the face gear drive with a helical pinion.

Compared with the face gear drive with a helical pinion, the change in the angle of the shaft in the face gear drive with a spur pinion does not affect the meshing area of the tooth surface, but the change in the angle of the shaft affects the contact force of the tooth surface, thereby affecting the contact temperature. It can be seen from the calculation results that increasing the angle of the shaft makes the contact temperature increase, and this is more obvious near the top of the tooth and at the root of the face gear tooth. When the shaft angle is less than 90°, the contact temperature of the face gear drive with a spur pinion will be slightly smaller than that of the face gear drive with a helical pinion, and when the shaft angle is greater than 90°, the contact temperature of the face gear drive with a helical pinion will be slightly larger than that of the face gear drive with a spur pinion. It can be seen that the reasonable geometric parameter selection has a greater effect on the anti-gluing design of the face gear.

6. Conclusions

An analytical model is established to predict the surface contact temperature of face gear drives. According to the Blok flash temperature theory, the instantaneous surface contact temperature calculation model of the face gear is established, and the Gaussian distribution is used to describe the bulk temperature of the tooth surface. The analytical model is verified by FEA. The comparison error between the two calculation results is within 9.1%. On the premise of ensuring the calculation accuracy, the surface contact temperature is solved effectively and efficiently. Through the study of the influence of the geometric parameters on the surface contact temperature, it can be found that the pressure angle has the greatest influence on the surface contact temperature. The helix angle and shaft angle have large influences on the temperature of the contact area near the root and can change the position of the lowest surface contact temperature at the tooth surface, and the tooth width has little effect on the surface contact temperature. It can be seen that, under certain working conditions, reasonable selection of the geometric parameters of the face gear can improve the anti-scuffing bearing capacity of the face gear.

Author Contributions: Conceptualization, J.W. and Y.Z.; methodology, Y.Z.; software, J.W.; validation, J.T. and Y.D.; investigation, J.W.; data curation, J.T.; writing—original draft preparation, J.W.; writing—review and editing, Y.Z.; visualization, J.W.; supervision, Y.D.; project administration, J.T.; funding acquisition, Y.Z. and J.T. All authors have read and agreed to the published version of the manuscript.

Funding: This research was funded by Hunan Provincial Natural Science Foundation of China (No. 2021JJ20071) and the science and technology innovation Program of Hunan Province (No. 2021RC3012) and the National Natural Science Foundation of China through Grant No. 52075558.

Data Availability Statement: All data that support the findings of this study are included within the article.

Acknowledgments: The authors gratefully acknowledge the support of Hunan Provincial Natural Science Foundation of China (No. 2021JJ20071) and the science and technology innovation Program of Hunan Province (No. 2021RC3012) and the National Natural Science Foundation of China through Grant No.52075558.

Conflicts of Interest: The authors declare no conflict of interest.

Nomenclature

ϕ	rotation angle
N	tooth number
M	homogenous transformation matrix
r	shaper tooth surface
n	normal of the shaper tooth surface
v	velocity of the shaper tooth surface
d	partial derivatives
H	mean curvature
K	Gaussian curvature
$\Delta\gamma_m$	error of the shaft angle
ΔE	offset of the pinion
Δq	axial displacement of the face gear
S	coordinate system
θ_{fla}	flash temperature of the contact point
μ	friction coefficient
F_{n}	normal load
v_{t}	tangential relative sliding velocity
B	thermal contact coefficient
b	half-width of the Hertz contact band
h_0	center distance of the two contact rigid bodies
R_{x}	radius of curvature in the direction of the minor axis of the contact ellipse
R_{y}	radius of curvature in the direction of the major axis of the contact ellipse
V	amount of elastic deformation of the contact surface
E^*	effective elastic modulus
ρ	density
h	oil film thickness between the interfaces
p	pressure
η^*	effective viscosity of the lubricating oil
η	lubricant viscosity
τ_0	reference shear stress
τ_L	limiting shear stress
τ	shear stress
γ	shear rate of lubricant
f_c	boundary friction
F_f	mixed traction force
λ	heat transfer coefficient
c	specific heat
ξ	radius of curvature
k	principal curvature
α	angle between the main direction of the pinion and the major axis of the contact ellipse
σ	angle between the pinion and the first main direction of the face gear
θ_{m}	tooth surface temperature
θ_{oil}	operating temperature of lubricating oil
X_{S}	lubrication conditions coefficient
Γ	contact path dimensionless parameter
θ_{b}	bulk temperature
K_a	temperature coefficient
Q	heat flux
H_i	convection heat transfer coefficients
Nu_i	Nusselt number
L	characteristic length of boundary surface

References

1. Litvin, F.L.; Fuentes, A. *Gear Geometry and Applied Theory*; Cambridge University Press: Cambridge, UK, 2004.
2. Litvin, F.L.; Zhang, Y.; Wang, J.C.; Bossler, R.B.; Chen, Y.J.D. Design and geometry of face-gear drives. *J. Mech. Des.* **1992**, *114*, 642–647. [CrossRef]

3. Litvin, F.L.; Wang, J.C.; Bossler, J.R.B.; Chen, Y.J.D.; Heath, G.; Lewicki, D.G. Application of Face-Gear Drives in Helicopter Transmissions. *J. Mech. Des.* **1994**, *116*, 672–676. [CrossRef]
4. Litvin, F.L.; Egelja, A.; Tan, J.; Chen, Y.D.; Heath, G. *Handbook on Face Gear Drives with a Spur Involute Pinion*; NASA: Location, UK, 2000.
5. Litvin, F.L.; Egelja, A.; Tan, J.; Heath, G. Computerized design, generation and simulation of meshing of orthogonal offset face-gear drive with a spur involute pinion with localized bearing contact. *Mech. Mach. Theory* **1998**, *33*, 87–102. [CrossRef]
6. Litvin, F.L.; Gonzalez-Perez, I.; Fuentes, A.; Vecchiato, D.; Hansen, B.D.; Binney, D. Design, generation and stress analysis of face-gear drive with helical pinion. *Comput. Methods Appl. Mech. Eng.* **2005**, *194*, 3870–3901. [CrossRef]
7. Litvin, F.L.; Fuentes, A.; Howkins, M. Design, generation and TCA of new type of asymmetric face-gear drive with modified geometry. *Comput. Methods Appl. Mech. Eng.* **2001**, *190*, 5837–5865. [CrossRef]
8. Litvin, F.L.; Nava, A.; Fan, Q.; Fuentes, A. New geometry of face worm gear drives with conical and cylindrical worms: Generation, simulation of meshing, and stress analysis. *Comput. Methods Appl. Mech. Eng.* **2002**, *191*, 3035–3054. [CrossRef]
9. Tang, Z.; Zhou, Y.; Wang, S.; Zhu, J.; Tang, J. An innovative geometric error compensation of the multi-axis CNC machine tools with non-rotary cutters to the accurate worm grinding of spur face gears. *Mech. Mach. Theory* **2022**, *169*, 104664. [CrossRef]
10. Wang, S.; Hu, B.; Wu, Z.; Zhou, Y.; Tang, J. A Comprehensive Optimization Model of Tooth Surface Parameters for the Minimization of Contact Stress of Helical Face Gears by Considering the Avoidance of Edge Contact. *Mathematics* **2022**, *10*, 3102. [CrossRef]
11. Liu, D.; Wang, G.; Ren, T. Transmission principle and geometrical model of eccentric face gear. *Mech. Mach. Theory* **2017**, *109*, 51–64. [CrossRef]
12. Wu, Y.; Zhou, Y.; Zhou, Z.; Tang, J.; Ouyang, H. An advanced CAD/CAE integration method for the generative design of face gears. *Adv. Eng. Softw.* **2018**, *126*, 90–99. [CrossRef]
13. Zhou, Y.; Wu, Y.; Wang, L.; Tang, J.; Ouyang, H. A new closed-form calculation of envelope surface for modeling face gears. *Mech. Mach. Theory* **2019**, *137*, 211–226. [CrossRef]
14. Zhou, Y.-S.; Tang, Z.-W.; Shi, X.-L.; Tang, J.-Y.; Li, Z.-M.-Q. Efficient and accurate worm grinding of spur face gears according to an advanced geometrical analysis and a closed-loop manufacturing process. *J. Cent. South Univ.* **2022**, *29*, 1–13. [CrossRef]
15. Lu, X.; Zhou, Y.; He, D.; Zheng, F.; Tang, K.; Tang, J. A novel two-variable optimization algorithm of TCA for the design of face gear drives. *Mech. Mach. Theory* **2022**, *175*, 104960. [CrossRef]
16. Guo, H.; Peng, X.; Zhao, N.; Zhang, S. A CNC grinding method and envelope residual model for face gear. *Int. J. Adv. Manuf. Technol.* **2015**, *79*, 1689–1698. [CrossRef]
17. Guo, H.; Gonzalez-Perez, I.; Fuentes-Aznar, A. Computerized generation and meshing simulation of face gear drives manufactured by circular cutters. *Mech. Mach. Theory* **2019**, *133*, 44–63. [CrossRef]
18. Wang, S.; Zhou, Y.; Chu, C.-H.; Tang, J. Novel kinematic and geometric views for improving tooth contact analysis of spatial gears. *J. Comput. Des. Eng.* **2022**, *9*, 1076–1096. [CrossRef]
19. Zhou, Y.; Wang, S.; Wang, L.; Tang, J.; Chen, Z.C. CNC milling of face gears with a novel geometric analysis. *Mech. Mach. Theory* **2019**, *139*, 46–65. [CrossRef]
20. Yang, X.Y.; Tang, J.Y. Research on manufacturing method of CNC plunge milling for spur face-gear. *J. Mater. Process. Technol.* **2014**, *214*, 3013–3019. [CrossRef]
21. Tang, J.; Yang, X. Research on manufacturing method of planing for spur face-gear with 4-axis CNC planer. *Int. J. Adv. Manuf. Technol.* **2016**, *82*, 847–858. [CrossRef]
22. Shen, Y.B.; Liu, X.; Li, Z.P.; Li, D.Y. Research on shaving processing of spiroid face gear. *Int. J. Adv. Manuf. Technol.* **2017**, *92*, 605–613. [CrossRef]
23. Wang, Y.; Lan, Z.; Hou, L.; Chu, X.; Yin, Y. An efficient honing method for face gear with tooth profile modification. *Int. J. Adv. Manuf. Technol.* **2017**, *90*, 1155–1163. [CrossRef]
24. Hölm, B.R.; Miclwelis, K.; Collenberg, H.; Schlenk, L. Effect of temperature on the scuffing load capacity of EP gear lubricants. *Tribotest* **2001**, *7*, 317–332. [CrossRef]
25. Zhang, J.-G.; Liu, S.-J.; Fang, T. Determination of surface temperature rise with the coupled thermo-elasto-hydrodynamic analysis of spiral bevel gears. *Appl. Therm. Eng.* **2017**, *124*, 494–503. [CrossRef]
26. Gan, L.; Xiao, K.; Wang, J.; Pu, W.; Cao, W. A numerical method to investigate the temperature behavior of spiral bevel gears under mixed lubrication condition. *Appl. Therm. Eng.* **2019**, *147*, 866–875. [CrossRef]
27. Fernandes, C.M.C.G.; Rocha, D.M.P.; Martins, R.C.; Magalhães, L.; Seabra, J.H.O. Finite element method model to predict bulk and flash temperatures on polymer gears. *Tribol. Int.* **2018**, *120*, 255–268. [CrossRef]
28. Li, W.; Zhai, P.; Tian, J.; Luo, B. Thermal analysis of helical gear transmission system considering machining and installation error. *Int. J. Mech. Sci.* **2018**, *149*, 1–17. [CrossRef]
29. Mohammadpour, M.; Theodossiades, S.; Rahnejat, H.; Dowson, D. Non-Newtonian mixed thermo-elastohydrodynamics of hypoid gear pairs. *Proc. Inst. Mech. Eng. Part J J. Eng. Tribol.* **2017**, *232*, 1105–1125. [CrossRef]
30. Wang, K.L.; Cheng, H.S. A Numerical Solution to the Dynamic Load, Film Thickness, and Surface Temperatures in Spur Gears, Part I: Analysis. *J. Mech. Des.* **1981**, *103*, 177–187. [CrossRef]
31. Zhu, D.; Cheng, H.S. An Analysis and Computational Procedure for EHL Film Thickness, Friction and Flash Temperature in Line and Point Contacts. *Tribol. Trans.* **1989**, *32*, 364–370. [CrossRef]

32. Bobach, L.; Beilicke, R.; Bartel, D.; Deters, L. Thermal elastohydrodynamic simulation of involute spur gears incorporating mixed friction. *Tribol. Int.* **2012**, *48*, 191–206. [CrossRef]
33. Li, W.; Tian, J. Unsteady-state temperature field and sensitivity analysis of gear transmission. *Tribol. Int.* **2017**, *116*, 229–243. [CrossRef]
34. Blok, H. The flash temperature concept. *Wear* **1963**, *6*, 483–494. [CrossRef]
35. ISO/TR 13989-1: 2000(en). Calculation of Scuffing Load Capacity of Cylindrical, Bevel and Hypoid Gears: Part 1: Flash Temperature Method. International Organization for Standardization: Geneva, Switzerland, 2000; pp. 1–39.
36. Pu, W.; Wang, J.; Zhang, Y.; Zhu, D. A theoretical analysis of the mixed elastohydrodynamic lubrication in elliptical contacts with an arbitrary entrainment angle. *J. Tribol.* **2014**, *136*, 041505. [CrossRef]
37. Zhu, D.; Hu, Y.Z. A computer program package for the prediction of ehl and mixed lubrication characteristics, friction, subsurface stresses and flash temperatures based on measured 3-d surface roughness. *Tribol. Trans.* **2001**, *44*, 383–390. [CrossRef]
38. Pu, W.; Wang, J.; Zhu, D. Friction and flash temperature prediction of mixedlubrication in elliptical contacts with arbitrary velocity vector. *Tribol. Int.* **2016**, *99*, 38–46. [CrossRef]
39. Pisaturo, M.; Senatore, A. Simulation of engagement control in automotive dryclutch and temperature field analysis through finite element model. *Appl. Therm. Eng.* **2015**, *93*, 958–966. [CrossRef]
40. Wang, W.Z.; Hu, Y.Z.; Liu, Y.C.; Wang, H. Deterministic solutions and thermal analysis for mixed lubrication in point contacts. *Tribol. Int.* **2007**, *40*, 687–693. [CrossRef]
41. Hu, Y.Z.; Zhu, D. A full numerical solution to the mixed lubrication in point contacts. *J. Tribol.* **2000**, *122*, 1–9. [CrossRef]
42. Jaeger, J. Moving sources of heat and the temperature at sliding contacts. *J. Proc. R. Soc. N. S. W.* **1942**, *76*, 203–224. [CrossRef]
43. Shi, Y.; Yao, Y.-P.; Fei, J.-Y. Analysis of bulk temperature field and flash temperature for locomotive traction gear. *Appl. Therm. Eng.* **2016**, *99*, 528–536. [CrossRef]
44. Holman, J.P. Heat exchangers. *Heat Transf.* **2010**, *1*, 521–587.